Thermomechanical noise limits on parametric sensing with nanomechanical resonators

A N Cleland

Department of Physics, University of California at Santa Barbara,
Santa Barbara, CA 93106, USA

Abstract. Measuring and monitoring the dynamic parameters of a nanomechanical resonator, in particular the resonance frequency, has received significant attention recently, in part due to the possibility of very sensitive, fast and precise mass sensing. Added mass can include chemisorbed or physisorbed metals or organic molecules, and if sufficiently high sensitivity, dynamic range and detector speed can be achieved, they could have applications in, e.g., proteomics. Here, I investigate some of the fundamental limits to mass sensing in such resonators, discussing the limits imposed by thermomechanical noise on both the linear operating regime of a simple harmonic oscillator, and the equivalent limits on nonlinear parametric amplifiers used as parametric sensors. The model system is a cantilevered flexural resonator, but the results apply equally well (in most cases) to doubly clamped or torsional resonant structures as well.

Contents

The very small mass of nanomechanical resonators, ranging from nanograms for atomic force microscope-style cantilevers, to sub-picogram masses for structures with dimensions below $1\,\mu$m, combined with their high-intrinsic quality factor Q, makes such devices very appealing for applications, such as mass sensing [1]–[5]. A precise monitoring of the natural resonance frequency $\omega_0 = \sqrt{k/m}$ of a simple harmonic oscillator will detect a change of $\Delta\omega/\omega_0 = -\Delta m/2m$ due to an added mass Δm, so a system with a minimum frequency resolution $\Delta\omega_{min}$ can detect a minimum added mass of $\Delta m_{min} = 2m\Delta\omega_{min}/\omega_0$. Small resonator masses m and high resonance frequencies ω_0 naturally lend themselves to very small detection limits. The precision $\Delta\omega$ with which the frequency can be measured is determined in part by the quality factor Q of the resonator, which determines the natural linewidth as well as the intrinsic thermomechanical noise in the system. In any actual implementation, other important limits are imposed by the frequency stability of the measuring system, as well as environmental issues such as the temperature stability, but here we focus on the intrinsic limit set by the thermomechanical noise due to finite Q. We examine both the limits for a linear harmonic oscillator, and for a parametrically modulated oscillator, as in this latter system, a much narrower resonant response to an external driving force can be achieved than that set by the quality factor of the system [6, 7]. In either case, the physical system is a cantilevered beam on whose surface the mass to be detected is placed.

1. Linear parametric sensing

In figure 1, we display the model system for this paper, a cantilevered beam of length L, width w and thickness t, oriented along the x-axis, driven into flexural resonance with displacement along the y-axis.

1.1. Mechanics of a cantilevered beam

Euler–Bernoulli theory [8, 9] applies to such a structure when the aspect ratio $L/t \gg 1$, for small amplitudes of motion. In the absence of dissipation, the transverse displacement $Y(x, t)$ of the cantilever centreline (along the y-direction) obeys the differential equation

$$\rho w t \frac{\partial^2 Y}{\partial t^2}(x, t) = -\frac{\partial^2}{\partial x^2} E I \frac{\partial^2 Y}{\partial x^2}(x, t), \tag{1}$$
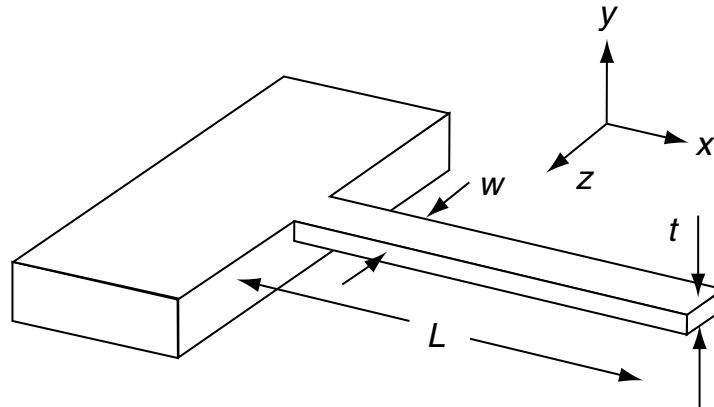
Figure 1. Cantilevered beam with length L, width w and thickness t. The fixed end is at $x = 0$ and the free end at $x = L$. Motion is along the y-axis, and the end support at $x = 0$ is assumed infinitely rigid.

where $I = wt^3/12$ is the bending moment of inertia, ρ the material density and E the Young's modulus. The end at $x = 0$ is clamped, that at $x = L$ is free, so that the boundary conditions [9] are $Y(x = 0) = Y'(x = 0) = 0$ and $Y''(L) = Y'''(L) = 0$. The solutions to (1) have the form

$$Y_n(x, t) = [a_n(\cos \beta_n x - \cosh \beta_n x) + b_n(\sin \beta_n x - \sinh \beta_n x)] \exp(-i\Omega_n t), \quad (2)$$

with the eigenvalues β_n satisfying $\cos \beta_n L \cosh \beta_n L = -1$, with solutions $\beta_n L = 1.875, 4.694, 7.855, 10.996 \ldots$. The frequencies Ω_n are the natural resonance frequencies of the cantilever; here we will focus on the motion at the fundamental frequency $\nu_1 = \Omega_1/2\pi$, where

$$\nu_1 = \frac{\Omega_1}{2\pi} = 0.162\sqrt{\frac{E}{\rho}}\frac{t}{L^2}. \quad (3)$$

With total resonator mass $m = \rho wtL$, this can be written as

$$\nu_1 = \frac{1}{2\pi}\sqrt{\frac{k_{\text{eff}}}{m}}, \quad (4)$$

with effective spring constant $k_{\text{eff}} = 1.036\,Ewt^3/L^3 = \Omega_1^2 m$.

The mutually orthogonal eigenfunctions Y_n in (2) are chosen to be normalized to the beam length, so that

$$\int_0^L Y_n(x)Y_m(x)\,\mathrm{d}x = L^3\delta_{mn}. \quad (5)$$

The corresponding coefficients for the $n = 1$ mode are $a_1 = -L$ and $b_1 = 0.73411L$. An arbitrary solution $Y(x, t)$ to undriven or driven motion can be written as

$$Y(x, t) = \sum_{n=1}^{\infty} c_n(t)Y_n(x), \quad (6)$$

where the amplitudes c_n are dimensionless.

Dissipation can be included phenomenologically using the Zener model for damping [9, 10], by introducing the quality factor Q for the resonator material and replacing the Young's modulus by a phenomenological Young's modulus $E \rightarrow E_{eff}(1 + i/Q)$, which yields the damped form for the resonator motion given by (1)

$$\omega^2 \rho w t Y(x) = E_{eff} I \left(1 + \frac{i}{Q}\right) \frac{\partial^4 Y}{\partial x^4}(x). \tag{7}$$

The spatial solutions $Y(x)$ are the same as for (1), but the dispersion relation giving the damped eigenfrequencies ν'_n in terms of the undamped frequencies ν_n is

$$\nu'_n = \frac{\Omega'_n}{2\pi} = \left(1 + \frac{i}{2Q}\right)\nu_n \tag{8}$$

for small dissipation Q^{-1}. The imaginary part of ν'_n implies that the nth eigenmode will decay in amplitude as $\exp(-\Omega_n t/2Q)$.

We now add a harmonic driving force $F(x, t) = f \exp(i\omega_c t)$, where f is the position-independent force per unit length. The force is uniform across the beam cross-section and directed along y-axis, and the carrier frequency ω_c is close to Ω_1. The equation of motion is given by [8]

$$\rho \frac{\partial^2 Y}{\partial t^2} + E_{eff}\left(1 + \frac{i}{Q}\right)\frac{\partial^4 Y}{\partial x^4} = \frac{f}{wt}e^{i\omega_c t}. \tag{9}$$

For ω_c close to Ω_1, and waiting long enough for the transients to die out, only the $n = 1$ term in (6) has a significant amplitude, with amplitude given by

$$c_1 = \frac{\eta_1}{\Omega_1^2 - \omega_c^2 + i\,\Omega_1^2/Q}\frac{f}{m}, \tag{10}$$

where $\eta_1 = 0.7829$ and the corresponding displacement of the beam is $Y(x, t) = c_1 Y_1(x)\exp(i\omega_c t)$. The on-resonance amplitude, for $\omega_c = \Omega_1$ and high Q, is $c_1 = -i\eta_1 Qf/m\Omega_1^2$, lagging the force by $90°$.

The linear response represented by (10) holds for small amplitudes c_1. A practical limit to the amplitude is when $c_1 \approx 1$, when the end displacement $y_{max} = c_1 Y_1(x = L) = 2L$, which occurs for a driving force per unit length $f = m\Omega_1^2/\eta_1 Q$.

In the absence of noise, the solution (10) represents pure harmonic motion at the carrier frequency ω_c, with a fixed, time-invariant amplitude $y_{max} = 2c_1 L$. However, the nonzero values of Q^{-1} and temperature T necessitates the presence of noise, from the fluctuation–dissipation theorem. This acts to thermalize the motion of the resonator, so that the amplitude acquires a time dependence, $c(t) = c_1 + c_n(t)$, where the mean energy of the noise amplitude $c_n(t)$, $\langle E_n \rangle$, is equal to $k_B T$, where T is greater than or equal to the physical temperature of the resonator [11, 12].

1.2. Noise in the cantilevered beam

Thermalization occurs due to the presence of a noise force $f_N(x, t)$ per unit length of the beam, with white spectral density. The spectral density of the resulting noise-driven amplitude $y_n(t)$ of

the fundamental mode is given by

$$S_n(\omega) = \frac{4L^2}{(\Omega_1^2 - \omega^2)^2 + (\Omega_1^2/Q)^2} \frac{S_f(\omega)}{m^2}. \tag{11}$$

In the thermal limit, the noise spectral density S_f is given by

$$S_f(\omega) = \frac{2k_B Tm\Omega_1}{\pi Q L^2}. \tag{12}$$

A one-dimensional simple harmonic oscillator has the equivalent thermal force density $S_F(\omega) = 2k_B Tm\Omega/\pi Q$. The spectral density of the amplitude noise that results from (12) is

$$S_n(\omega) = \frac{\Omega_1}{(\Omega_1^2 - \omega^2)^2 + (\Omega_1^2/Q)^2} \frac{8k_B T}{\pi m Q}. \tag{13}$$

The amplitude noise $y_n(t)$ can equivalently be regarded as 'phase' noise. The phase noise power density $S_\phi(\omega)$ at frequency ω from the carrier frequency is given by [10]

$$S_\phi(\omega) = \frac{1}{2} \frac{S_n(\Omega_1 + \omega)}{4L^2|c_1|^2} = \frac{\Omega_1}{(2\Omega_1\omega + \omega^2)^2 + (\Omega_1^2/Q)^2} \frac{k_B T}{\pi |c_1|^2 L^2 m Q}. \tag{14}$$

For frequencies well off the peak resonance, $\omega \gg \Omega_1/Q$, but small compared to the resonance frequency, $\omega \ll \Omega_1$, this may be written as

$$S_\phi(\omega) \approx \frac{1}{4\pi\varepsilon_c Q} \left(\frac{\Omega_1}{\omega}\right)^2 \quad (\Omega_1/Q \ll \omega \ll \Omega_1). \tag{15}$$

Here, we define $\varepsilon_c = m\Omega_1^2 L^2 |c_1|^2/k_B T = k_{\text{eff}} L^2 |c_1|^2/k_B T$, the energy of motion in units of the thermal energy. This can be written in terms of frequency $f = 2\pi\omega$ as

$$S_\phi(f) \approx \frac{1}{2\varepsilon_c Q} \left(\frac{\nu_1}{f}\right)^2 \quad (\nu_1/Q \ll f \ll \nu_1). \tag{16}$$

The phase noise can equivalently be viewed as frequency fluctuations, where the amplitude $c(t)$ has a time dependence given by the carrier frequency ω_c with a modulation $\delta\omega(t) = \mathrm{d}\phi/\mathrm{d}t$

$$c(t) = c_0 \sin\left\{\int_{-\infty}^{t} [\omega_c + \delta\omega(t)]\,\mathrm{d}t' + \theta\right\}. \tag{17}$$

We consider a single-phase modulation component, so that $\phi(t) = \phi_0 \sin(\omega t)$. The frequency variation is then

$$\delta\omega(t) = \delta\omega_0 \cos(\omega t) = \omega\phi_0 \cos(\omega t). \tag{18}$$
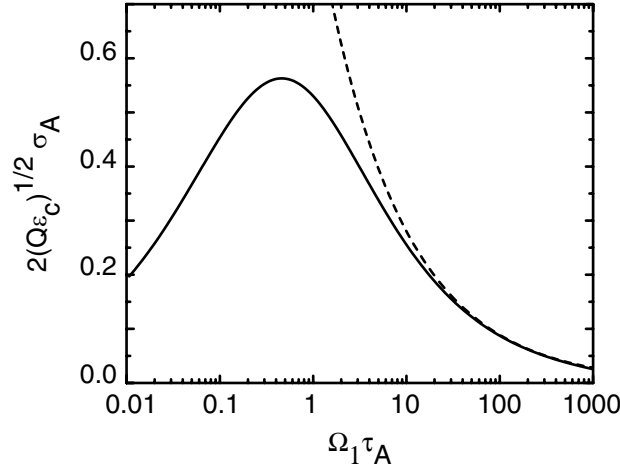
Figure 2. Dependence of the Allan variance σ_A on the dimensionless time interval $\Omega_1\tau_A$; the Allan variance has been scaled to remove the overall dependence on Q and on drive energy $\varepsilon_c = k_{\text{eff}}L^2/k_BT$. The full dependence from (14) is plotted as a solid line, while the approximate form (21) is plotted as a dotted line.

The frequency fluctuations can be quantified by the dimensionless Allan variance $\sigma_A(\tau_A)$ [10, 13, 14], defined as the variance over time in the measured frequency

$$\sigma_A^2(\tau_A) = \frac{1}{2f_c^2} \frac{1}{N-1} \sum_{m=2}^{N} (\bar{f}_m - \bar{f}_{m-1})^2, \tag{19}$$

where $\bar{f}_m$ is the average frequency measured over the mth time interval, of length $\Delta t = \tau_A$, and f_c is the carrier frequency. The squared Allan variance is related to the phase noise density $S_\phi(\omega)$ by [14]

$$\sigma_A^2(\tau_A) = 2\left(\frac{2}{\omega_c\tau_A}\right)^2 \int_0^\infty S_\phi(\omega) \sin^4(\omega\tau_A/2) \, \mathrm{d}\omega, \tag{20}$$

where $\omega_c = 2\pi f_c$ and ω is the modulation frequency.

For the approximate form for the phase noise density (16), the Allan variance is

$$\sigma_A(\tau_A) = \frac{1}{2}\sqrt{\frac{1}{\varepsilon_c Q\Omega_1\tau_A}}. \tag{21}$$

The Allan variance falls inversely with the square root of the measurement time τ_A, and is proportional to the square root of the dissipation $Q^{-1/2}$. Other things being equal, increasing the resonator frequency Ω_1 lowers the Allan variance.

In figure 2, we display the approximate result (21) as a function of $\Omega_1\tau_A$, scaled to remove the dependence on Q and on P_c; we also show the full result obtained from integrating (14), for values of $Q > 100$; for values of Q less than this, the calculated value for the scaled variance falls below the plotted values. We see that the approximate expression given by (21) works quite well for averaging times τ_A more than a few tens of the oscillation period $2\pi/\Omega_1$.

Table 1. Parameters for the resonators considered in this calculation. The resonators are assumed to be made of silicon, with $\rho = 2330 \, \mathrm{kg \, m^{-3}}$ and $E = 1.69 \times 10^{11} \, \mathrm{N \, m^{-2}}$.

L (μm)	t (μm)	w (μm)	m	ν_1
0.5	0.05	0.05	2.91 fg	276 MHz
5	0.5	0.5	2.91 pg	27.6 MHz
50	0.5	0.5	29.1 pg	27.1 kHz

1.3. Mass sensing

The addition of a small mass δm at one point on the resonator surface will change the resonator's natural resonance frequencies ν_n. The degree of change will depend on where along the length of the resonator the mass is placed, with the largest change at the beam midpoint. Here, we assume for simplicity that the mass adds uniformly to the mass of the overall resonator and then changes the fundamental resonance frequency by an amount $\delta\nu_1$ given by

$$\delta\nu_1 = \frac{\mathrm{d}\nu_1}{\mathrm{d}m}\delta m = \frac{1}{2}\frac{\delta m}{m}\nu_1. \tag{22}$$

The detection of small masses clearly is improved by using small resonator masses m and large resonator frequencies ν_1. However, the ability to detect such a change is limited by the natural fluctuations in resonator frequency, as quantified by the Allan variance. Here, we take the simple rule that the minimum detectable change is that which gives a fractional change in frequency equal to the Allan variance, $\delta\nu_1/\nu_1 = \sigma_A$, or

$$\frac{\delta m}{m} = 2\frac{\delta\nu_1}{\nu_1} = 2\sigma_A = \sqrt{\frac{k_B T}{k_{\mathrm{eff}} L^2}\frac{1}{Q\Omega_1\tau_A}}. \tag{23}$$

We can calculate what the detectable mass limits are for different resonator geometries, temperatures and quality factors, using (23). We consider three different resonator geometries, ranging from roughly atomic force microscope cantilever dimensions to the smallest dimensions that can easily be made using top-down lithographic processing. The three resonators are enumerated in table 1.

The minimum mass sensitivities of these resonators are plotted in figure 3, as a function of the resonator Q, ranging from 10^3 to 10^6, all calculated at room temperature. Reducing the temperature to liquid helium temperatures yields a factor of eight improvement in the mass sensitivity, scaling as $T^{1/2}$.

Clearly, the potential for single-proton detection is within reach for the smallest resonator at room temperature, even with relatively poor Q. Larger cantilevers can also achieve the same performance level at sufficiently high Q or if operated cryogenically. For practical applications of these devices to, e.g., proteomics, short measurement times are needed; if we assume a measurement time $\tau_A = 1$ ms, then the smallest cantilever in figure 3 could achieve single-proton sensing if a Q of about 1000 can be achieved, and if the thermomechanical noise is the dominant noise source.
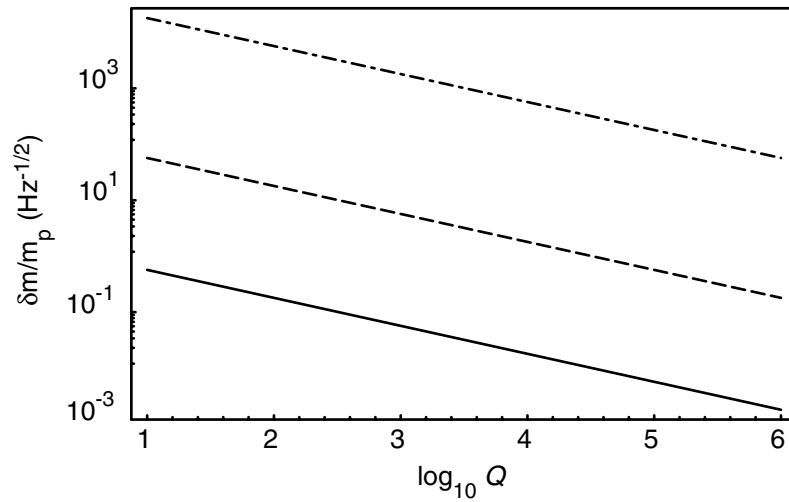
Figure 3. Minimum detectable mass using three different cantilever geometries, ranging in length from $0.5\,\mu$m (——) to $5\,\mu$m (– – –) to $50\,\mu$m (–·–·–·–). Mass is taken in units of the proton mass m_p per root Hz averaging time. All at room temperature.

2. Nonlinear parametric sensing

We now turn to a discussion of whether better sensitivity can be achieved using a parametric amplifier, again based on a cantilevered geometry such as that shown in figure 1. We base our calculation on the simple harmonic oscillator model for the cantilever vibration, where the transverse displacement $y(t)$ at the free end of the cantilever is treated as a single degree of freedom, with total effective mass m and spring constant k_{eff}, the latter chosen to yield the actual resonance frequency $\Omega_1^2 = k_{\text{eff}}/m$ of the cantilevered resonator. In addition, however, we add to the dynamic equation of motion, a modulation of the spring constant $k_m(t)$ that is externally controlled. Such a modulation can be achieved in practice using, e.g. a capacitive coupling between the cantilever and an external voltage source, as described by Rugar and Grütter [15].

Parametric amplification is achieved in this system by modulating k_m at *twice* the resonance frequency Ω_1 of the system. The advantage of using parametric amplification is that, as the modulation $k_m(t)$ is increased in amplitude, the response of the resonator to a weak external driving force $F(t)$ (e.g. a signal to be detected) is significantly amplified for drive frequencies near the resonance frequency Ω_1. The resonance width is also significantly narrowed, so that for parametric sensing the determination of the frequency appears to be improved over that of a simple harmonic oscillator system. Here, we investigate the noise limitations to this approach, calculating the phase noise and Allan variance for a parametric oscillator driven near its first critical point (see below).

2.1. Mechanics of parametric sensing

The equation of motion for the parametric oscillator is given by

$$m\frac{\mathrm{d}^2 y}{\mathrm{d}t^2} + \frac{m\Omega_1}{Q}\frac{\mathrm{d}y}{\mathrm{d}t} + [k_{\text{eff}} + k_m(t)]\,y = F(t). \tag{24}$$

This equation can be re-written using the Louisell transformations for a parametric electronic system [15, 16]. We define the complex resonance frequency ω_1 as

$$\omega_1 = \Omega_1 \left[\sqrt{1 - \frac{1}{4Q^2}} + \frac{\mathrm{i}}{2Q} \right]. \tag{25}$$

Note that $|\omega_1|^2 = \Omega_1$, $\omega_1 + \omega_1^\star = 2\Omega_1(1 - 1/4Q^2)^{1/2}$, and $\omega_1 - \omega_1^\star = \mathrm{i}\Omega_1/Q$.

The Louisell transformations are from y and $\mathrm{d}y/\mathrm{d}t$ to a complex variable a, defined as

$$\begin{cases} a = \dfrac{\mathrm{d}y}{\mathrm{d}t} + \mathrm{i}\omega_1^\star y, \\ a^\star = \dfrac{\mathrm{d}y}{\mathrm{d}t} - \mathrm{i}\omega_1 y. \end{cases} \tag{26}$$

The inverse transformations are

$$\begin{cases} y = -\mathrm{i}\dfrac{a - a^\star}{\omega_1^\star + \omega_1}, \\ \dfrac{\mathrm{d}y}{\mathrm{d}t} = \dfrac{\omega_1 a + \omega_1^\star a^\star}{\omega_1^\star + \omega_1}. \end{cases} \tag{27}$$

The equation of motion in terms of a is then

$$\frac{\mathrm{d}a}{\mathrm{d}t} = \mathrm{i}\omega_1 a + \mathrm{i}\frac{k_m(t)}{m}\frac{a - a^\star}{\omega_1^\star + \omega_1} + \frac{F(t)}{m}. \tag{28}$$

We drive the system with the external drive $F(t) = F_0 \cos(\omega_d t + \phi)$, with a parametric modulation at twice the drive frequency, $k_m(t) = \Delta k \sin(2\omega_d t)$. We assume that the solutions to the equation of motion have the form $a(t) = A\mathrm{e}^{\mathrm{i}\omega_d t} + B\mathrm{e}^{-\mathrm{i}\omega_d t}$, including only the fundamental drive frequency. Inserting this in the equation of motion (28) yields the intermediate result

$$\mathrm{i}(\omega_d - \omega_1)A\mathrm{e}^{\mathrm{i}\omega_d t} - \mathrm{i}(\omega_d + \omega_1)B\mathrm{e}^{-\mathrm{i}\omega_d t} = \frac{\Delta k}{2m(\omega_1 + \omega_1^\star)}[(A - B^\star)(\mathrm{e}^{3\mathrm{i}\omega_d t} - \mathrm{e}^{-\mathrm{i}\omega_d t})$$

$$+ (B - A^\star)(\mathrm{e}^{\mathrm{i}\omega_d t} - \mathrm{e}^{-3\mathrm{i}\omega_d t})] + \frac{F_0}{2m}(\mathrm{e}^{\mathrm{i}\omega_d t + \mathrm{i}\phi} + \mathrm{e}^{-\mathrm{i}\omega_d t - \mathrm{i}\phi}). \tag{29}$$

In the high-Q limit, we keep only the terms at the fundamental frequency $\pm\omega_d$, which yields the equations

$$\mathrm{i}(\omega_d - \omega_1)A = \frac{\Delta k}{2m(\omega_1 + \omega_1^\star)}(B - A^\star) + \frac{F_0}{2m}\mathrm{e}^{\mathrm{i}\phi},$$

$$-\mathrm{i}(\omega_d + \omega_1)B = -\frac{\Delta k}{2m(\omega_1 + \omega_1^\star)}(A - B^\star) + \frac{F_0}{2m}\mathrm{e}^{-\mathrm{i}\phi}. \tag{30}$$

Defining the dimensionless variables $\tilde{A} = 2m\Omega_1 A/F_0 = \tilde{A}_r + \mathrm{i}\tilde{A}_i$ and $\tilde{B} = 2m\Omega_1 B/F_0 = \tilde{B}_r + \mathrm{i}\tilde{B}_i$, we approximate where appropriate $\omega_1 + \omega_1^\star \approx 2\Omega_1$ and $\omega_d + \omega_1 \approx \omega_d + \Omega_1$. We define the parameter $\alpha = \Delta k/4m\Omega_1^2 = \Delta k/4k_{\mathrm{eff}}$, and make the frequency dimensionless through

$z = \omega_d / \Omega_1$, ultimately yielding the dimensionless set of equations

$$\begin{cases} (z-1)\tilde{A}_r + \dfrac{1}{2Q}\tilde{A}_i &= \alpha(\tilde{A}_i + \tilde{B}_i) + \sin\phi, \\[2mm] -(z-1)\tilde{A}_i + \dfrac{1}{2Q}\tilde{A}_r &= \alpha(\tilde{B}_r - \tilde{A}_r) + \cos\phi, \\[2mm] -(z+1)\tilde{B}_r &= -\alpha(\tilde{A}_i + \tilde{B}_i) - \sin\phi, \\[2mm] (z+1)\tilde{B}_i &= -\alpha(\tilde{A}_r - \tilde{B}_r) + \cos\phi. \end{cases} \tag{31}$$

For $z = \omega_d / \Omega_1$ close to the resonance value of 1, within the natural resonance width of the resonator, $\tilde{A}$ completely dominates over $\tilde{B}$, and the latter can be neglected. For frequencies more than 2 or 3 times the natural width of the resonance, however, the magnitude of $\tilde{A}$ and $\tilde{B}$ are comparable, and ignoring the counter-rotating term is not a good approximation.

For z near 1, we neglect $\tilde{B}$, leaving

$$\begin{cases} (z-1)\tilde{A}_r + \dfrac{1}{2Q}\tilde{A}_i &= \alpha\tilde{A}_i + \sin\phi, \\[2mm] -(z-1)\tilde{A}_i + \dfrac{1}{2Q}\tilde{A}_r &= -\alpha\tilde{A}_r + \cos\phi. \end{cases} \tag{32}$$

Exactly on resonance, at $z = 1$, these resolve to

$$\begin{cases} \tilde{A}_r &= \dfrac{2Q\cos\phi}{1 + 2\alpha Q}, \\[3mm] \tilde{A}_i &= \dfrac{2Q\sin\phi}{1 - 2\alpha Q}, \end{cases} \tag{33}$$

bringing out the overall nature of the response as a function of the modulation parameter α. As α increases from zero, $\tilde{A}_i$ increases and $\tilde{A}_r$ decreases. There is a critical value $\alpha_c = 1/2Q$, where $\tilde{A}_i$ diverges to infinity; beyond that modulation value, the system bifurcates to one with two resonances, close to $z = 1$, but separating in frequency as α increases past α_c (this latter behaviour is not apparent from (33), but can be seen by solving the full z-dependent equations (32)).

We can extract the displacement dependence from these results, using the inverse transformation $y(t) \approx \text{Im}\, a(t)/\Omega_1$

$$y(t) = \frac{F_0}{2m\Omega_1^2}[(\tilde{A}_i + \tilde{B}_i)\cos\omega_d t + (\tilde{A}_r - \tilde{B}_r)\sin\omega_d t]. \tag{34}$$

For frequencies near resonance

$$y(t) \approx \frac{F_0}{2k_{\text{eff}}}(\tilde{A}_i \cos\omega_d t + \tilde{A}_r \sin\omega_d t). \tag{35}$$

Exactly on resonance, at $z = 1$, this is

$$y(t) \approx \frac{QF_0}{k_{\text{eff}}}\left(\frac{\sin\phi}{1 - 2\alpha Q}\cos\omega_d t + \frac{\cos\phi}{1 + 2\alpha Q}\sin\omega_d t\right). \tag{36}$$
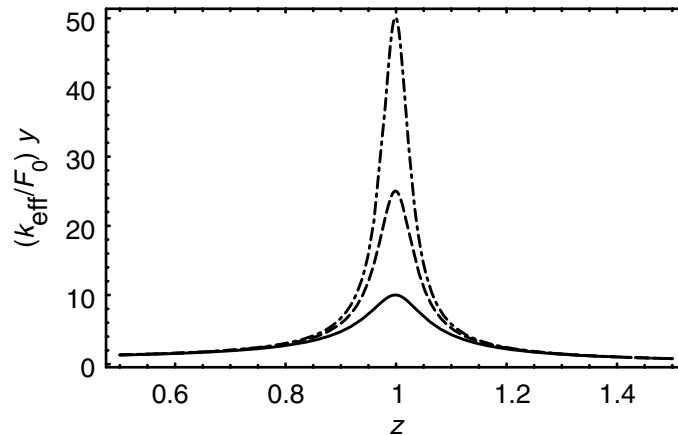
Figure 4. Displacement amplitude as a function of frequency $z = \omega_d/\Omega_1$, for three values of the parametric modulation $\alpha = 0$ (———), 0.03 (– – –) and 0.04 (–·–·–·–). These are calculated with the phase $\phi = \pi/2$ and $Q = 10$. Displacement amplitude is plotted as $(k_{\mathrm{eff}}/F_0)\,y(t)$.
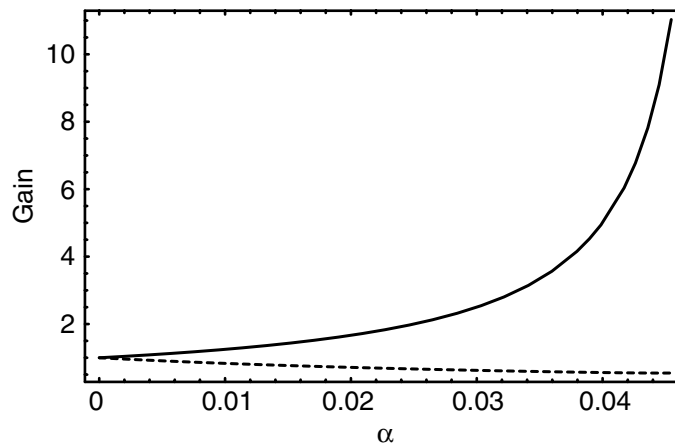
Figure 5. Gain as a function of parametric modulation α, for $\phi = 0$ (- - - -) and $\phi = \pi/2$ (———). Frequency $z = 1$ and $Q = 10$.

For $\alpha = 0$, the on-resonance displacement is $y(t) = Q\,F(t)/k_{\mathrm{eff}}$ (the simple harmonic oscillator result). For $\alpha \neq 0$, the displacement amplitude depends on the phase ϕ; for $\phi = 0$, the displacement is *smaller* than the simple harmonic oscillator result (at all frequencies), while for $\phi = \pi/2$, the displacement is always *larger*. The amplitude of motion is linear in the drive F_0, but as α increases the response diverges at the critical point. Here, we focus on the subcritical regime.

First we examine the displacement as a function of frequency for different values of α. This is shown in figure 4 for three values of α, using a resonator with quality factor $Q = 10$, although the same behaviour applies to higher natural Q values. The critical value is at $\alpha_c = 1/2Q = 0.05$.

In figure 5, we show the parametric gain $G(\alpha, \phi)$ as a function of the modulation α for different phase angles ϕ. The gain is defined, as in Rugar and Grütter [15], as the maximum displacement amplitude with modulation ($\alpha \neq 0$) divided by that with $\alpha = 0$, both calculated at
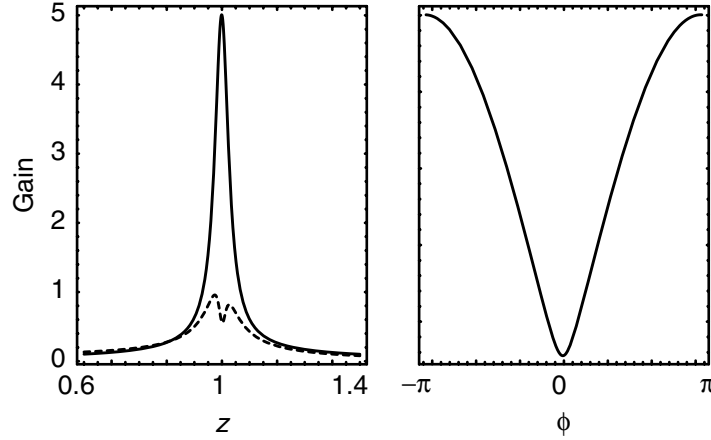
Figure 6. Left: gain as a function of frequency $z = \omega_d/\Omega_1$, with parametric modulation $\alpha = 0.04$, for $\phi = 0$ (- - - -) and $\phi = \pi/2$ (——). Right: gain as a function of phase angle ϕ, with frequency $z = 1$ and modulation $\alpha = 0.04$. Quality factor $Q = 10$.

the resonance frequency $z = 1$. Minimum gain is achieved when $\phi = 0$ and maximum gain for $\phi = \pi/2$. For $\phi = 0$, the gain is $G(\alpha, 0) = 1/(1 + 2\alpha Q)$, reaching a minimum at the critical value $\alpha_c = 1/2Q$ of $G(\alpha_c, 0) = 1/2$. For $\phi = \pi/2$, the gain is $G(\alpha, \pi/2) = 1/(1 - 2\alpha Q)$, diverging as $\alpha \to \alpha_c$.

In figure 6, we show the gain as a function of the drive frequency and phase, for a resonator with $Q = 10$.

2.2. Noise in a parametric oscillator

What effect does noise have on this system? We consider exclusively the subcritical regime and take into account only the thermomechanical noise due to the finite Q. The oscillator is driven at its natural resonance by a signal $F_0 \cos(\Omega_1 t + \phi_0)$ (with ϕ_0 held fixed at $\pi/2$ for maximum gain) and modulation $k_p(t) = \Delta k \sin(2\Omega_1 t)$. The spectral density of the noise force for a simple harmonic oscillator is $S_F(\omega) = 2k_B T m \Omega_1 / \pi Q$. The displacement $y(t)$ can be resolved into its quadrature phases, $y(t) = Y_c(t) \cos \Omega_1 t + Y_s(t) \sin \Omega_1 t$, where $Y_c(t)$ and $Y_s(t)$ are time-varying amplitudes, driven by noise about their average values Y_{c0} and Y_{s0}, the latter determined by F_0 and ϕ_0.

The spectral density $S_c(\omega)$ for fluctuations in the cosine displacement component Y_c is, averaging over the noise phase angle ϕ_n,

$$S_c(\omega) = \frac{2}{(2m\Omega_1^2)^2} \langle (\tilde{A}_i(1 + \omega/\Omega_1) + \tilde{B}_i(1 + \omega/\Omega_1))^2 \rangle_{\phi_n} S_F(\Omega_1 + \omega) \qquad (37)$$

$$\approx \frac{k_B T}{\pi k_{\text{eff}} Q \Omega_1} \langle \tilde{A}_i^2(1 + \omega/\Omega_1) \rangle_{\phi_n}, \qquad (38)$$

with the terms $\tilde{A}$ and $\tilde{B}$ evaluated at the dimensionless frequency $z = 1 + \omega/\Omega_1$, so that ω represents the offset from the centre frequency Ω_1. For the equivalent noise in the sine
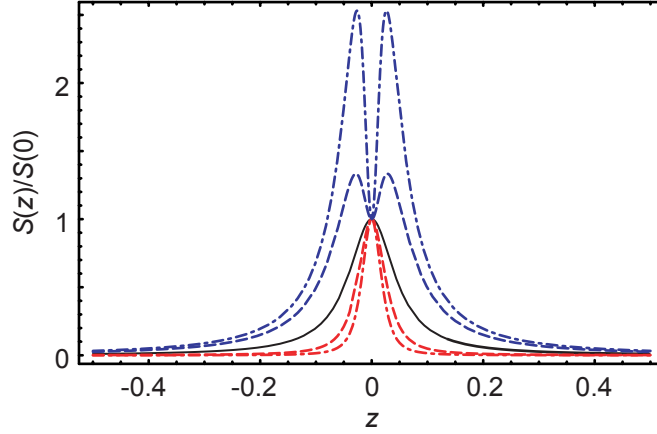
Figure 7. Noise powers $S_c(\omega)/S_c(0)$ (red) and $S_s(\omega)/S_s(0)$ (blue) for different values of $\alpha = 0$ (black), 0.03 (– – –) and 0.04 (–·–·–·–). Quality factor $Q = 10$.

component Y_s, we have

$$S_s(\omega) = \frac{2}{(2m\Omega_1^2)^2} \langle (\tilde{A}_r(1 + \omega/\Omega_1) - \tilde{B}_r(1 + \omega/\Omega_1))^2 \rangle_{\phi_n} S_F(\Omega_1 + \omega) \qquad (39)$$

$$\approx \frac{k_B T}{\pi k_{\mathrm{eff}} Q \Omega_1} \langle \tilde{A}_r^2(1 + \omega/\Omega_1) \rangle_{\phi_n}, \qquad (40)$$

where in the second approximation we drop $\tilde{B}$ in favour of $\tilde{A}$.

For offset frequencies $\omega \approx 0$, we can take the $z = 1$ result for $\tilde{A}$ and find

$$\begin{cases} S_c(\omega \approx 0) & \approx & \dfrac{2Q k_B T}{\pi k_{\mathrm{eff}} \Omega_1} \dfrac{1}{(1 - 2\alpha Q)^2}, \\[3mm] S_s(\omega \approx 0) & \approx & \dfrac{2Q k_B T}{\pi k_{\mathrm{eff}} \Omega_1} \dfrac{1}{(1 + 2\alpha Q)^2}, \end{cases} \qquad (41)$$

having averaged over the noise phase angles ϕ_n.

We see that for frequencies close to zero (i.e. slow fluctuations in $Y_{c,s}$), the noise in the cosine quadrature is amplified by the square of the gain $G(\alpha, \pi/2)$, while the noise in the sine quadrature is reduced by the square of $G(\alpha, 0)$; the maximum reduction is a factor of 4 in noise power.

For frequencies offset from zero, we use the results for $\tilde{A}_r$ and $\tilde{A}_i$ from (32). The overall scale of the response follows that given by (41), but with a more complex frequency dependence. In figure 7, we display the frequency dependence for $S_c(\omega)$ and $S_s(\omega)$, for different values of α. Both of the noise powers are normalized to their values at $z = 1$ ($\omega = 0$).

Note that S_c becomes narrower as α increases, and that the noise power at $\omega = 0$ increases faster than that off-resonance. In contrast, S_s becomes broader, and the noise off-resonance does not decrease as quickly as that on-resonance, making the scaled plots at larger α grow in comparison to those for $\alpha = 0$.

The phase noise corresponding to the displacement noise is

$$S_\phi(\omega) = \frac{1}{2} \frac{S_c(\omega) + S_s(\omega)}{|Y_{c0}|^2 + |Y_{s0}|^2}, \qquad (42)$$

where Y_{c0} and Y_{s0} are the displacement amplitudes from the driving force F_0. The interesting limit is where the modulation approaches the critical value α_c, which is where $S_c(\omega)$ dominates the noise, and where Y_{c0} (the cosine-driven term) dominates over Y_{s0}. In this limit $S_\phi(\omega) \approx S_c(\omega)/2|Y_{c0}|^2$.

The zero-offset displacement noise can be written as $S_c(0) = (2k_BTk_{\mathrm{eff}}/\pi\Omega_1 Q)(|Y_{c0}|/F_0)^2$, independent of α. Hence, the noise on resonance is amplified by the same amount as the square displacement. The parametric amplifier does not select signal to noise, and thus does not improve signal-to-noise on-resonance (or off-resonance). Hence, we can write the phase noise as

$$S_\phi(\omega) \approx \frac{k_BTk_{\mathrm{eff}}}{\pi\Omega_1 Q F_0^2}\frac{S_c(\omega)}{S_c(0)}, \tag{43}$$

with a frequency dependence identical to that in figure 7. The force F_0 and modulation α ultimately are limited by a maximum displacement $Y_{c0} \approx L$, which corresponds to $F_{0,\mathrm{max}} = k_{\mathrm{eff}}L(1 - 2\alpha Q)/Q$.

We can calculate the Allan variance from the phase noise as

$$\sigma_A^2(\tau_A) = 2\left(\frac{2}{\Omega_1\tau_A}\right)^2 \int_0^\infty S_\phi(\omega) \sin^4(\omega\tau_A/2)\,\mathrm{d}\omega \tag{44}$$

$$\approx \frac{8k_BTk_{\mathrm{eff}}}{\pi Q F_0^2}\frac{1}{u^2}\int_0^\infty \frac{S_c(z)}{S_c(0)}\sin^4(uz/2)\,\mathrm{d}z \tag{45}$$

with $u = \Omega_1\tau_A$. With the maximum force limited by amplitude considerations, the minimum Allan variance is

$$\sigma_{A,\mathrm{min}}(\tau_A) = \sqrt{\frac{4}{\pi Q}\frac{k_BT}{k_{\mathrm{eff}}L^2}I_A(u)}, \tag{46}$$

with dimensionless integral is given by

$$I_A(u) = \frac{1}{u^2}\int_0^\infty \langle \tilde{A}_i^2(1+z)\rangle_{\phi_n}\sin^4(uz/2)\,\mathrm{d}z. \tag{47}$$

This can be compared with the simple harmonic oscillator result (21). Note that the Allan variance depends on the integral $I_A(u)$ through the relative thermal to motional energy scale as well as the quality factor, but that all the dependence on the parametric modulation α is contained in the integral. In figure 8, we display the dependence of the Allan variance integral I_A for different α, for $Q = 10$.

Here, we find a surprising result: at short averaging times (large frequencies), the Allan variance integral is independent of the parametric modulation α, while at long averaging times, where the noise close to the carrier is sampled, the Allan variance becomes *worse* with increasing parametric amplification. For short sampling times, $u\Omega_1\tau_A < 1/Q$, the noise is dominated by the off-resonant, unamplified noise, and does not change with the amplification. The surprising result that the amplification makes the variance worse is due to the scaling of the maximum applicable force F_0, which becomes smaller as α increases due to the increased amplification. If one instead uses a *fixed* force F_0, set small enough so that at the largest $\alpha < \alpha_c$, the maximum displacement remains less than the beam length, the noise improves with increasing α. However,
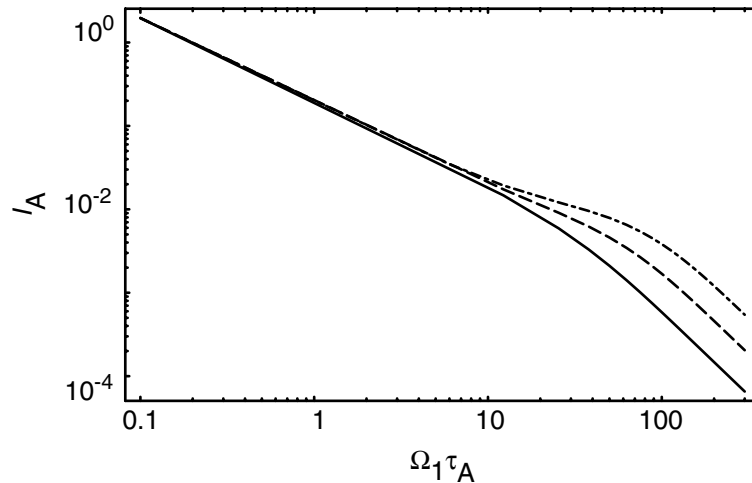
Figure 8. Integral $I_A(u)$ from (47), calculated for $\alpha = 0$ (——), 0.03 (– – –) and 0.04 (–·–·–·–). Quality factor $Q = 10$.

as the overall variance is reduced if the maximum possible force amplitude F_0 is used, this is not a fair comparison. Hence, the best performance is achieved for *zero* parametric amplification, i.e. for a linear simple harmonic oscillator.

We note that the form of the integral for small u in figure 8 does not match that for small u in figure 2 for $\alpha = 0$; this is because we are using the approximation such that $\tilde{B}$ can be neglected, which is not very accurate for large frequencies z, corresponding to small averaging times u in figure 2. Using the full expression involving both $\tilde{A}$ and $\tilde{B}$ in the integral for S_ϕ gives the same result, for $\alpha \to 0$, as for the linear harmonic oscillator.

3. Conclusions

We summarize the results here by the following simple statement: the highest sensitivity, highest measurement bandwidth in mass-sensing applications of nanomechanical resonators, is achieved for the smallest resonators that can be fabricated with the smallest aspect ratio L/t, operated at the lowest practicable temperatures with the highest achievable Q. Even at room temperature, with moderate quality factors $Q \approx 1000$, and reasonable ($\sim$ millisecond) averaging times, single-proton sensitivity can be achieved with relatively easily fabricated cantilever dimensions. However, we also arrive at the surprising result that parametric amplification does not give improved performance over that achieved in the linear regime.

Acknowledgments

Institute *of* **Physics** Φ DEUTSCHE PHYSIKALISCHE GESELLSCHAFT

References

[1] Ekinci K L, Huang X M H and Roukes M L 2004 Ultrasensitive nanoelectromechanical mass detection *Appl. Phys. Lett.* **84** 4469–71

[2] Ilic B, Craighead H G, Krylov S, Senaratne W, Ober C and Neuzil P 2004 Attogram detection using nanoelectromechanical oscillators *J. Appl. Phys.* **95** 3694–703

[3] Ilic B, Yang Y and Craighead H G 2004 Virus detection using nanoelectromechanical devices *Appl. Phys. Lett.* **85** 2604–6

[4] Ghatkesar M K, Barwich V, Braun T, Bredekamp A H, Drechsler U, Despont M, Lang H P, Hegner M and Gerber Ch 2004 Real-time mass sensing by nanomechanical resonators in fluid *Proc. IEEE Sensors 2004* 1060–3

[5] Ghatnekar-Nilsson S, Forsen E, Abadal G, Verd J, Campabadal F, Perez-Murano F, Esteve J, Barniol N, Boisen A and Montelius L 2005 Resonators with integrated cmos circuitry for mass sensing applications, fabricated by electron beam lithography *Nanotechnology* **16** 98–102

[6] Turner K L, Miller S A, Hartwell P G, MacDonald N C, Strogatz S H and Adams S G 1998 Five parametric resonances in a microelectromechanical system *Nature* **396** 149–51

[7] Zalatudinov M, Olkhovets A, Zehnder A, Ilic B, Czaplewski D, Craighead H G and Parpia J M 2001 Optically pumped parametric amplification for micromechanical oscillators *Appl. Phys. Lett.* **78** 3142–4

[8] Timoshenko S, Young D H and Weaver W Jr 1974 *Vibration Problems in Engineering* (New York: Wiley)

[9] Cleland A N 2002 *Foundations of Nanomechanics* (Berlin: Springer)

[10] Cleland A N and Roukes M L 2002 Noise processes in nanomechanical resonators *J. Appl. Phys.* **92** 2758–68

[11] Albrecht T R, Grütter P, Horne D and Rugar D 1991 Frequency modulation detection using high-Q cantilevers for enhanced force noise microscope sensitivity *J. Appl. Phys.* **69** 668–73

[12] Gabrielson T B 1993 Mechanical and thermal noise in micromechanical acoustic and vibration sensors *IEEE Trans. Electron Devices* **40** 903–9

[13] Allan D W 1966 Statistics of atomic frequency standards *Proc. IEEE* **54** 221–30

[14] Egan W F 1981 *Frequency Synthesis by Phase Lock* (New York: Wiley)

[15] Rugar D and Grütter P 1991 Mechanical parametric amplification and thermomechanical noise squeezing *Phys. Rev. Lett.* **67** 699–702

[16] Louisell W H 1960 *Coupled Mode and Parametric Electronics* (New York: Wiley)